SN 2005bf: A Transition Event Between Type Ib/c Supernovae and Gamma Ray Bursts

Gastón Folatelli[1], Carlos Contreras[1], M. M. Phillips[1], S. E. Woosley[2], Sergei Blinnikov[3], Nidia Morrell[1,12], Nicholas B. Suntzeff[4], Brian L. Lee[5], Mario Hamuy[1,10], Sergio González[1], Wojtek Krzeminski[1], Miguel Roth[1], Weidong Li[6], Alexei V. Filippenko[6], W. L. Freedman[7], Barry F. Madore[7,8], S. E. Persson[7], David Murphy[7], Samuel Boissier[7], Gaspar Galaz[9], Luis González[10], P. J. McCarthy[7], Andrew McWilliam[7], Wojtek Pych[11]

ABSTRACT

We present $u'g'r'i'BV$ photometry and optical spectroscopy of the Type Ib/Ic SN 2005bf covering the first ∼100 days following discovery. The $u'g'BV$ light curves displayed an unprecedented morphology among Type Ib/Ic supernovae, with an initial maximum some 2 weeks after discovery, and a second, main maximum about 25 days after that. The bolometric light curve indicates that SN 2005bf was a remarkably luminous event, radiating at least 6.3×10^{42} erg s^{-1} at maximum light, and a total of 2.1×10^{49} erg during the first 75 days after the explosion. Spectroscopically, SN 2005bf underwent a unique transformation

[1]Las Campanas Observatory, Carnegie Observatories, Casilla 601, La Serena, Chile

[2]Department of Astronomy, University of California, Santa Cruz, CA 95064

[3]MPA D-85741 Garching, Germany, and ITEP 117218 Moscow, Russia

[4]Cerro Tololo Inter-American Observatory, Casilla 603, La Serena, Chile

[5]Department of Astronomy and Astrophysics, University of Toronto, 60 St. George St., Toronto, Ontario, Canada M5S 3H8

[6]Department of Astronomy, University of California, Berkeley, CA 94720-3411

[7]Observatories of the Carnegie Institution of Washington, 813 Santa Barbara St., Pasadena, CA 91101

[8]Infrared Processing and Analysis Center, Caltech/Jet Propulsion Laboratory, Pasadena, CA 91125

[9]Departamento de Astronomía y Astrofísica, Pontificia Universidad Católica de Chile, Casilla 306, Santiago 22, Chile

[10]Universidad de Chile, Departamento de Astronomía, Casilla 36-D, Santiago, Chile

[11]Copernicus Astronomical Center, Bartycka 18, PL-00716 Warszawa, Poland

[12]Member of the Carrera del Invstigador Científico, CONICET, Argenina; on leave from Facultad de Ciencias Astronómicas y Geofísicas, Universidad Nacional de La Plata

from a Type Ic-like event at early times to a typical Type Ib supernova at later phases. The initial maximum in $u'g'BV$ was accompanied by the presence in the spectrum of high velocity ($> 14,000$ km s^{-1}) absorption lines of Fe II, Ca II, and H I. The photospheric velocity derived from spectra at early epochs was below 10,000 km s^{-1}, which is unusually low compared with ordinary Type Ib supernovae. We describe one-dimensional computer simulations which attempt to account for these remarkable properties. The most favored model is that of a very energetic (2×10^{51} erg), asymmetric explosion of a massive (8.3 $M_\odot$) Wolf-Rayet WN star that had lost most of its hydrogen envelope. We speculate that an unobserved relativistic jet was launched producing a two-component explosion consisting of 1) a polar explosion containing a small fraction of the total mass and moving at high velocity, and 2) the explosion of the rest of the star. At first, only the polar explosion is observed, producing the initial maximum and the high velocity absorption-line spectrum resembling a Type Ic event. At late times, this fast-moving component becomes optically-thin, revealing the slower-moving explosion of the rest of the star and transforming the observed spectrum to that of a typical Type Ib supernova. If this scenario is correct, then SN 2005bf is the best example to date of a transition object between normal Type Ib/Ic supernovae and gamma ray bursts.

Subject headings: galaxies: individual (MCG +00-27-5) — supernovae: general — supernovae: individual (SN 2005bf)

1. INTRODUCTION

After years of relative neglect, Type Ib/Ic supernovae (SNe) are today the object of considerable observational and theoretical attention. This boom is largely due to the discovery that certain gamma ray bursts (GRBs) are associated with highly energetic Type Ic events commonly referred to as "hypernovae" (e.g., see Stanek et al. 2005, and references therein). Note, however, that this term has been expanded by some authors to include essentially any Type Ic with inferred high luminosity or unusually broad lines, whether or not it was associated with a GRB.

It is universally agreed that Type Ib/Ic SNe, as well as the transitional Type IIb SNe, are produced by the core collapse of a massive star which has lost most or all of its hydrogen envelope before exploding. Taken together as a class, the light curves of Type Ib/Ic/IIb SNe display a significant range in luminosities and morphologies, although there are subclasses of events which are relatively homogeneous in their properties (Clocchiatti & Wheeler 1997).

Unfortunately, only a handful of Type Ib/Ic SNe have been observed significantly before maximum, and so little is known of their photometric and spectroscopic properties at the earliest epochs following outburst.

At the Las Campanas Observatory, we have embarked on a multi-year observational program — the Carnegie Supernova Program (CSP) — to obtain follow-up photometry and spectroscopy of supernovae of all types (see Hamuy et al. 2005b, hereafter **Paper I**). One of the many goals of this project is to obtain uniform, high-precision observations of nearby Type Ib/Ic/IIb SNe in order to improve our knowledge of the optical and near-infrared characteristics of these explosions. Highest priority is given to SNe discovered soon after outburst, since it is at these early epochs where the largest range in photometric and spectroscopic properties is likely to be observed.

One of the first Type Ib/Ic events to be studied in detail as part of the CSP was SN 2005bf, which was independently discovered on 2005 April 6 by L. A. G. Monard at the Bronberg Observatory in South Africa, and by M. Moore and W. Li from the Lick Observatory Supernova Search (LOSS) (Monard, Moore, & Li 2005). The SN was located $11''.7$ east and $32''.6$ south of the nucleus of MCG +00-27-5, an SB galaxy with a recession velocity of 5,670 km s^{-1} (Falco et al. 1999). According to Monard, nothing was visible at the position of the SN on an unfiltered image taken on March 12 with limiting magnitude of 18.5. Moore and Li report no detection to a limiting unfiltered magnitude of 19.5 on an image from March 15, and a marginal detection at 18.8 on March 30. It was likely, therefore, that the explosion occurred between March 15-29.

Initial CSP spectroscopy revealed that SN 2005bf was a Type Ic event (Morrell et al. 2005), and optical photometry confirmed that the SN had, indeed, been caught on the rising part of the light curve. An intensive program of follow-up photometric and spectroscopic observations was initiated which unexpectedly revealed an unusual preliminary rise and fall in the u', g', B, and V light curves preceding by $\sim$25 days the main maxima in these bands (Hamuy et al. 2005a). Spectroscopy reported just before the time of the main maximum also revealed that SN 2005bf had transformed into a Type Ib or transitional Type IIb event with strong He I lines (Wang & Baade 2005).

In this paper, we present the CSP observations of SN 2005bf, and discuss these in the context of possible models of the star that produced this peculiar and, thus far, unique explosion.

2. PHOTOMETRY

Most of our optical photometry was obtained with the Swope 1-m telescope at the Las Campanas Observatory (LCO), using a SITe CCD and a set of Sloan Digital Sky Survey (SDSS) $u'g'r'i'$ and Johnson BV filters. We read a section of 1200×1200 pixels from the CCD, which, at a scale of $0.''435$ pixel^{-1}, yielded a field of view of $8.''7\times8.''7$. Typical image quality ranged between $1''$ and $2''$ (FWHM). A photometric sequence of comparison stars in the SN field was calibrated with the Swope telescope from observations of standard stars during four photometric nights. Figure 1 shows the SN field and the selected comparison stars. Table 1 lists the average $u'g'r'i'BV$ magnitudes derived for these stars. SN magnitudes in the standard SDSS+Johnson system were obtained differentially relative to the comparison stars using point-spread-function (psf) photometry. On every image, a psf was fitted to the SN and comparison stars within a radius of $3''$. We refer to **Paper I** for further details about the instrument and measurements.

Five unfiltered LOSS images obtained with the 0.8-m Katzman Automatic Imaging Telescope (KAIT) were included in our analysis because they allow us to study the very early stages of the SN. After some experimentation we found that the unfiltered instrumental magnitudes of the local standards could be satisfactorily transformed with a simple additive zero-point to the r' standard system with a dispersion $\lesssim$0.05 mag. The comparison of the resulting LOSS magnitudes of the SN on April 15 (JD ∼2,453,475; r' = 17.419) and 16 (JD ∼2,453,476; r' = 17.426) with those obtained with the Swope telescope on the same nights (r' = 17.409, and 17.406, respectively) confirms that the effective wavelength of the r' filter is a good match to that of the unfiltered bandpass. The first LOSS observation obtained on March 15 (JD ∼2,435,445), where the SN is not detectable, served to derive a lower limit to the SN magnitude of $r' > 20.0$ mag.

A 17-day gap in the r' and i' observations with the Swope telescope was partially filled with an r' image and a spectrum obtained on May 7 (JD ∼2,453,497) using the Low Dispersion Survey Spectrograph 3 (LDSS-3) at the Clay 6.5-m telescope at LCO. For this purpose, we used the filter response functions of r' and i' given by Smith et al. (2002) to compute a synthetic $(r' - i')$ color from the spectrum, and thence derive a synthetic i' magnitude from the observed r' magnitude.

The resulting $u'g'r'i'BV$ magnitudes of SN 2005bf and their uncertainties are listed in Table 2. A minimum uncertainty of 0.015 mag was assumed for a single measurement based on the typical scatter in the transformation from instrumental to standard magnitudes of bright stars (**Paper I**). Figure 2 shows the corresponding light curves. We computed K-corrections for the $g'r'i'BV$ filters (the u' passband lies beyond the coverage of our spectra) using the available spectra. Given the small redshift of the SN, the corrections proved small, within

± 0.02 mag in all cases. We therefore decided to neglect them in our analysis.

Errors in our photometry could potentially arise from a poor subtraction of underlying host galaxy light. Fortunately, SN 2005bf was located in an outer region of the galaxy (see Figure 1). Inspecting the pre-discovery template LOSS images, no strong background variations are found at the location of the SN within a radius of $\sim 3''$ or in the sky annulus. If the contamination was large, the seeing changes from epoch to epoch would cause a large variation in such contamination and, consequently, a large scatter in the light curves. The small scatter seen in the light curves (typically 0.01-0.03 mag) is an indication that the contamination must be very small.

As mentioned in § 1, the $u'g'BV$ light curves of SN 2005bf show a unique behavior consisting of a first maximum around April 13 (JD 2,453,474), a subsequent decline lasting several days, a second rise which brings the SN to a main maximum around May 8 (JD 2,453,498), and finally a 30-day fast decline phase followed by a slower decline phase. Although the $r'i'$ light curves do not show this double maximum they do show a shoulder around the time of the first maximum. The other remarkable feature is the long time ($\sim$40 days) in all filters the SN took to reach the main maximum. There is a large range in light curve width among Type Ib/Ic SNe (Hamuy 2004), with the "hypernovae" SN 1997ef and SN 1998bw having two of the broadest ones, but even these objects took between 15 and 20 days to reach maximum light (Galama et al. 1998; Iwamoto et al. 2000). Table 3 lists the dates of maximum and peak magnitudes for SN 2005bf in $u'g'r'i'BV$, and in the bolometric lightcurve (see § 4.2).

Figure 3 shows the SN colors along with the temperature derived from blackbody (BB) fits to the $g'r'i'BV$ magnitudes as described in § 4.2. All of the color curves track the temperature evolution very closely. We observe a temperature rise reaching 10,000 K at the time of the first maximum, a cooling phase for a period of 10 days which brings the temperature down to 7,300 K, a subsequent re-heating period of 13 days reaching 8,700 K close to the time of maximum luminosity, followed by a steady second cooling phase past maximum light.

In addition to the optical data, $YJHK_s$ photometry was obtained on three epochs using the Wide Field Infrared Camera (WIRC) and the Persson's Auxiliary Nasmyth Infrared Camera (PANIC) mounted on the duPont 2.5-m, and the Baade 6.5-m telescopes at LCO, respectively. Two comparison stars in the SN field were calibrated using observations of standard stars obtained on May 21 (JD $\sim$2,453,511) with the Baade 6.5-m telescope. Table 4 lists the $YJHK_s$ magnitudes for the comparison stars. SN magnitudes were computed differentially relative to the comparison stars with an aperture of $2''$ (see **Paper I**, for details). The $YJHK_s$ photometry for SN 2005bf is listed in Table 5. The quoted uncertainties assume a minimum error of 0.02 mag on an individual measurement (**Paper I**).

3. SPECTROSCOPY

A total of nine optical spectra were obtained using the long slit grism mode of the Wide Field Reimaging CCD Camera (WFCCD) at the duPont 2.5-m telescope and the LDSS-3 spectrograph at the Clay 6.5-m telescope, both at LCO. Table 6 gives a journal of the spectroscopic observations.

In general, the spectra were obtained using a narrow ($\sim$1-2$''$) slit oriented near the parallactic angle. The spectrum from May 31 (JD $\sim$2,543,521) was obtained through a wider (8.$''$65) slit. All the spectra were wavelength and flux calibrated using arc-lamp and flux standards observations (Hamuy et al. 1994). In some cases, a smooth spectrum star selected from Table 4 of Bessell (1999) was observed to correct for telluric absorption features (see **Paper I**).

Additionally, a spectrum of the underlying host galaxy near the location of the SN was extracted from the LDSS-3 observation of May 7 (JD $\sim$2,453,497). Several emission (Hα and [N II] $\lambda\lambda$6548, 6583) and absorption (Na I D1 & D2, and Ca II H & K) lines were identified, which allowed us to derive an average recession velocity at the location of the SN of 5,496 $\pm$ 27 km s^{-1}. This is somewhat lower than the recession velocity of 5,670 $\pm$ 8 km s^{-1} given by Falco et al. (1999) for the host galaxy, a difference probably due to the rotation of the galaxy. The former velocity was adopted to shift the observed wavelength axis of the spectra to the SN rest frame.

Figure 4 shows the series of SN spectra sorted in time. The main spectral features are labeled with the ions that produce them. The position of the two main telluric absorption features are marked with an Earth symbol. The numbers in parenthesis give the epoch of each spectrum in SN rest frame days since the time of maximum bolometric luminosity (JD = 2,453,499.8, see § 4.2). We will hereafter use these epochs to label the spectra.

4. ANALYSIS

4.1. Spectroscopic Analysis

SN 2005bf was classified by Morrell et al. (2005) as a Type Ic event due to the absence of strong H I and He I lines which are the distinguishing features of Type II and Ib SNe, respectively. Although the initial spectra of SN 2005bf showed a prominent absorption at $\sim$6250 Å that could be attributed to Si II λ6355, it was not nearly as strong as is observed in typical Type Ia SNe, nor was there any evidence in the spectra for the S II $\lambda\lambda$5454,5640 feature which is also prominent around maximum light in Type Ia SNe. The two topmost spectra shown in Figure 5 compare SN 2005bf (day −32) and the Type Ic SN 1994I five days before maximum light (Filippenko et al. 1995). The comparison shows that at early times, SN 2005bf could be classified as a Type Ic SN. A similar comparison of SN 2005bf with an early-time spectrum of SN 1987M led Modjaz, Kirshner, & Challis (2005) to independently classify SN 2005bf as a Type Ic event. As SN 2005bf evolved, however, the He I lines grew in strength, and as shown in the bottom of Figure 5, the spectra from day +21 and later became almost identical to those of the Type Ib SN 1984L. This transformation was also noticed by Wang & Baade (2005). Interestingly, as shown in the middle of Figure 5, the spectrum from day −20 (and also those from days −2 and +3) was remarkably similar to spectra of the intermediate Type Ib/Ic SN 1999ex obtained around maximum light (Hamuy et al. 2002).

Figure 4 indicates that the He I $\lambda\lambda$5876,6678,7065 lines were present, albeit weakly, in the first spectra of SN 2005bf, and grew steadily in strength during the period covered by our observations. The expansion velocities as measured from the absorption minima of these features were nearly constant at a value of ∼8,000-10,000 km s^{-1} for this entire period.

As a tool for analyzing the pre-maximum spectral evolution of SN 2005bf, we used the SYNOW code (Fisher 2000) to calculate synthetic spectral fits to our first five spectra. Following the precepts of Branch et al. (2002), we assumed a power-law radial density gradient of index $n = 8$ and a Boltzmann excitation temperature of $T_{exc} = 7,000$ K for all of these fits. In general, only the Fe II, Ca II, He I, and H I ions were included in the calculations. The fits were not intended to reproduce all the observed features but to provide support to the present analysis. The addition of other ions would not modify our conclusions. Figure 6 shows the final SYNOW fits overplotted on the observed spectra.

With the aid of the SYNOW fits we noticed that the conversion from a Type Ic to a Type Ib SN was accompanied by a sudden change in the expansion velocity of the absorption components of the Fe II $\lambda\lambda$4924,5018,5169 lines and the Ca II $\lambda\lambda$8498,8542,8662 triplet feature. The left half of Figure 7 shows that two separate components of the Fe II lines were present in the spectrum from day −24: one at an expansion velocity of ∼14,000 km s^{-1}, and the other at ∼8,000 km s^{-1}. In fact, low- and high-velocity components of Fe II and Ca II were identifiable as early as our first spectrum (day −32) with the aid of the SYNOW fits. At early epochs, a low-velocity Ca II component, weaker than its high velocity counterpart, helps to fit the red wing of the H & K absorption. Similarly, a low-velocity Fe II component added to the high-velocity one improves the fit in the region between 4500 Å and 5200 Å. The high-velocity component dominated the spectrum obtained on day −32, but had disappeared by day −2. The spectra from day −2 onward showed exclusively the low-velocity absorption component of Fe II and Ca II. This strongly suggests that the appearance of high-velocity

Fe II and Ca II lines is associated with the initial maximum exhibited by the $u'g'BV$ light curves. The evolution of the expansion velocities of these components is summarized in the right half of Figure 7.

During the period covered by our spectroscopic observations, we find that the low-velocity component of Fe II and Ca II decreased roughly monotonically between ∼10,000 and ∼6,000 km s^{-1}. We have identified this with the photospheric velocity in our SYNOW fits. Assuming this interpretation is correct, and that the expansion was spherically symmetric, the He I lines are most consistent with arising from a shell which has a maximum velocity of ∼11,000 km s^{-1}, whereas the high-velocity Fe II, Ca II, and Hα lines are produced in a detached shell at velocities ≥14,000 km s^{-1}.

The 6250 Å absorption, like the high-velocity Fe II and Ca II lines, was present at early epochs but disappeared by the time of maximum light. A similar feature has been seen in several Type Ib SNe and its identification is a long-debated issue (e.g., see Wheeler et al. 1994; Branch et al. 2002). We consider the most likely identification to be high-velocity (∼15,000 km s^{-1}) Hα for two basic reasons: 1) the coincidence in expansion velocity with the Fe II and Ca II lines which show a similar association with the peculiar initial maximum in the $u'g'BV$ light curves, and 2) the presence of a very weak absorption feature in the spectra from days −24 and −20 (marked with a dotted line in Figure 4) which could be identified as Hβ at the same expansion velocity and with a strength consistent with that predicted by SYNOW spectra[1]. We reject the alternative identification of this feature with Si II λ6355 since it would imply an expansion velocity of ∼4800 km s^{-1}, which is significantly lower than the photospheric velocity estimated at these early epochs[2]. We consider unlikely identifications with C II λ6580 or Ne I λ6402 for the same reasons given by Branch et al. (2002) for ordinary Type Ib SNe. Thus, a small amount of hydrogen appears to be present in the outer ejecta of SN 2005bf.

Finally, we note that none of the spectra presented here shows the narrow or intermediate-width emission lines caused by an interaction between the ejecta and any preceding slow circumstellar wind, as observed in Type IIn events (Schlegel 1990).

---

[1]According to Wang & Baade (2005), weak absorption consistent with Hβ and Hγ was also present in a spectrum obtained on Apr 30 (day −9).

[2]Nevertheless, we cannot rule out that the absorption is produced by a blend of high-velocity Hα with Si II λ6355 at 8,000-10,000 km s^{-1}.

4.2. Bolometric Light Curve

The $u'g'r'i'BV$ photometry was used to compute a quasi-bolometric light curve covering the wavelength range from $\lambda = 3000$-∞ Å. Our broad-band magnitudes were corrected for Galactic extinction using $E(B-V)_{\rm Gal} = 0.045$ (Schlegel, Finkbeiner, & Davis 1998) and the reddening law with $R_V = 3.1$ given by Cardelli, Clayton, & Mathis (1989). Additional extinction originating in the host galaxy is difficult to estimate. Examination of our spectrum from day -2, which has the best wavelength resolution and signal-to-noise, reveals the presence of interstellar absorption lines of Na I D1 & D2, and Ca II H & K at the redshift of the galaxy, suggestng that some extinction existed. However, the uncertainties in estimating $E(B-V)_{\rm Host}$ from the equivalent widths (EWs) of these lines are large. We measure the total EW of the Na I D1 & D2 lines to be 0.86 Å. According to Turatto, Benetti, & Cappellaro (2003), two values of the color excess would be favored: $E(B-V)_{\rm Host} = 0.1$ and 0.4, depending on the gas-to-dust ratio of the host galaxy environment. We consider the value $E(B-V)_{\rm Host} = 0.4$ to be unrealistic because it would imply color temperatures of $\sim$40,000 K during the time of initial maximum (see below). Such high temperatures do not agree with the ionic species observed in our spectra. Hence, the lower value of $E(B-V)_{\rm Host} = 0.1$ would seem more likely. Close examination of the day -2 spectrum reveals Na I D absorption due to our own Galaxy at an equivalent width of approximately $\sim$0.5 Å. If the interstellar medium in the host galaxy of SN 2005bf is similar to that of the Galaxy, this would also suggest an extinction of $E(B-V)_{\rm Host} \sim 0.1$. Given the uncertainties, we adopt $E(B-V)_{\rm Host} = 0.0$ for our analysis, but present the case of $E(B-V)_{\rm Host} = 0.1$ as an alternative.

The extinction corrected $u'g'r'i'BV$ broad-band magnitudes were converted into monochromatic fluxes at the effective wavelengths of 3557, 4825, 6261, 7672, 4448, and 5505 Å, respectively, as given by Fukugita et al. (1996, their Tables 2a and 2c). On epochs where a certain filter observation was not available, its magnitude was interpolated in time from the light curve using the surrounding points and a low order polynomial. The total "uvoir" flux $F_{u' \to i'}$ in the region between the effective wavelengths of the u' and i' filters was integrated using the trapezoid approximation. On the blue side of 3557 Å the flux $F_\nu(3557)$ derived from the u' magnitude was extrapolated with a straight line to zero flux at 3000 Å (the blueward limit of the u' filter), and no significant flux was supposed to be emitted at shorter wavelengths, an assumption based on observations of other Type Ib/Ic SNe and of SN 1987A (Panagia 2003). On the infrared side the flux was extrapolated to $\lambda = \infty$ using a blackbody (BB) model obtained by fitting the $g'r'i'BV$ fluxes with a Planck function (shifted to the rest frame of the SN)[3]. The integrated flux under the fitted Planck function between

[3]The u' points were excluded from the BB fits because they clearly departed from the model, especially

the effective wavelength of the i' filter and $\lambda = \infty$ was taken as the IR correction. This correction remained below 35% of the total flux until a few days after maximum light and increased to 60% thereafter. A by-product of this procedure is the color temperature (T_{bb}) obtained from the BB fits. The values of T_{bb} for $E(B-V)_{\rm Host} = 0.0$ are given in Table 2 and shown in Figure 3 along with the observed SN colors[4]. The sum of $F_{u' \rightarrow i'}$ and the UV and IR corrections yielded the bolometric flux $F_{\rm bol}$.

Both $F_{u' \rightarrow i'}$ and $F_{\rm bol}$ were then transformed into uvoir ($L_{u' \rightarrow i'}$) and bolometric luminosity ($L_{\rm bol}$), respectively, using a distance of 83.8±10.2 Mpc based on the Hubble law, a value of the Hubble constant of $H_0 = 72 \pm 8$ km s^{-1} Mpc^{-1} (Freedman et al. 2001), and a recession velocity in the cosmic microwave background frame of 6,032 ± 300 km s^{-1}. The resulting luminosities computed with $E(B-V)_{\rm Host} = 0.0$ are listed in Table 2, and the bolometric light curves of SN 2005bf are shown in Figure 8 for both $E(B-V)_{\rm Host} = 0.0$ (filled circles) and $E(B-V)_{\rm Host} = 0.1$ (dashed line). The uvoir luminosities are shown with a dotted line. The luminosity correspoding to JD 2,453,565.5 is plotted with an error bar between 4.6 and 5.4×10^{41} erg s^{-1} owing to the large uncertainties in the $r'i'$ magnitudes.

Four late-time observations obtained with the Swope 1-m telescope between JD 2,453,538 and 2,453,570 involved only the BV filters. In those cases, integration of the flux in the optical range using the trapezoid approximation was not possible. Instead, bolometric luminosities were computed by determining bolometric corrections ($M_{\rm bol} - V$) from ($B-V$) colors. A linear relation with a scatter of ∼0.03 mag was found between these two quantities in the range $0.5 < (B-V) < 1.1$. The $(B-V)$ colors for the late-time epochs lie in the range from 1.04 to 1.18. The relation above was used to derive the $L_{\rm bol}$ values listed in parentheses in Table 2. Figure 8 shows these values with open circles and error bars derived by propagating the uncertainties in $(B-V)$.

The observations obtained between 30-70 days after maximum bolometric luminosity indicate late-time decline rates of 0.032 ± 0.009 mag day^{-1} in B, 0.034 ± 0.004 mag day^{-1} in V, and 0.038 ± 0.002 mag day^{-1} in $M_{\rm bol}$. These values are significantly larger than the decline rate of 0.0098 mag day^{-1} predicted if all the energy from the decay of ^{56}Co into ^{56}Fe was fully

before maximum light. The u' fluxes generally lay below the fitted BB curves, probably due to strong line blanketing in that part of the spectrum. The effect of including the u' would be to lower the derived BB temperature values. For consistency, we kept the same policy for post-maximum epochs, even though there was a better agreement of the u' fluxes with the fitted BB curves.

[4]As a further corroboration, we included the few NIR photometry points in the BB fits. This exercise showed an agreement within 10% between the bolometric flux based on u' through i' and that based on u' through K_s (or u' through H on JD 2,453,483.5). The BB fits showed a systematic increase in temperature of about 500 to 800 K when going from a range of B through i' to B through K_s.

thermalized in the ejecta (Woosley 1988), implying that at this epoch the ejecta of SN 2005bf did not trap all the γ-ray radiation.

The discovery LOSS images from March 30 (JD 2,453,459.8) and April 6 (JD 2,453,466.8) can be used to provide valuable information on the early rise of the bolometric light curve. We consider here the case of $E(B-V)_{\rm Host} = 0.0$. The r' magnitudes derived from the unfiltered images were converted to bolometric magnitudes ($M_{\rm bol}$) by extrapolating an average of the bolometric correction ($M_{\rm bol} - r'$) found for the first ten days of follow-up with the Swope telescope (JD 2,453,467.7 through 2,453,477.6) to the discovery epochs. The resulting bolometric luminosities are given in parentheses in Table 2, and are plotted with open squares in Figure 8. An uncertainty of 1.4×10^{41} erg s^{-1} in the bolometric luminosity of April 6 was estimated by summing in quadrature the photometric error in r' and an uncertainty of 0.1 mag in the adopted bolometric correction. In the case of March 30 the main source of error was the extrapolation of the bolometric correction. The uncertainty was estimated in this case by computing bolometric luminosities for BB curves of varying temperatures in the range 3,000 $< T_{bb} <$ 20,000 K, and passing through the r' flux point. This yielded an asymmetric error bar of $(2.50 < L_{\rm bol} < 7.15) \times 10^{41}$ erg s^{-1}.

A simple integration of the bolometric luminosity between 40 days before and 35 days after the time of maximum luminosity yields a total energy output of 2.1×10^{49} erg.

5. MODELS AND IMPLICATIONS

Although SN 2005bf eventually evolved to resemble a fairly typical Type Ib SN, both its photometric and spectroscopic evolution leading up to maximum light were unusual in several aspects:

- The initial maximum observed in the $u'g'BV$ light curves is, to our knowledge, without precedence in Type Ib/Ic light curves. Although it superficially resembles the shock outbreaks observed for the Type Ib/Ic SN 1999ex (Stritzinger et al. 2002) and the Type IIb SN 1993J (Richmond et al. 1994), in both of those cases the initial rise occurred very quickly ($<$ 2 days) whereas the first maximum in SN 2005bf ocurred at least two weeks following outburst. This much longer rise time argues strongly against it being due to shock outbreak.
- The bolometric light curve did not reach maximum until at least 40 days after outburst. Such a long rise time seems to be unique, although few Type Ib/Ic SNe have been caught early enough to be completely sure of this. We are aware of only two other

Type Ic events, the "hypernovae" SN 1997ef and SN 1998bw, which exhibited V light curves of comparable width although with shorter rise times (Galama et al. 1998; Iwamoto et al. 2000).

- SN 2005bf was also unusually luminous for a Type Ib/Ic SN, radiating 2.1×10^{49} erg in the 3000–∞ Å wavelength region during the first $\sim$75 days following outburst. This is nearly identical to the energy that we derived integrating the bolometric light curve of the "hypernova" SN 1998bw (Patat et al. 2001).

- The transformation from a Type Ic SN at early epochs to a Type Ib by maximum light is also unprecedented. However, we must point out that few Type Ib/Ic SNe have been observed spectroscopically at such early epochs. It should be noted that if SN 2005bf had not been discovered until maximum light, it would have been classified as a fairly typical Type Ib SN. This serves to emphasize the importance of observing SNe as soon as possible after outburst.

- The initial maximum in the $u'g'BV$ light curves was accompanied by the presence in the spectrum of high velocity absorption lines of Fe II, Ca II, and H I. This absorption had disappeared by the time of the principal maximum in the bolometric light curve, which argues for it being physically associated with the mechanism responsible for the initial maximum.

- The photospheric velocity of 9,000-10,000 km s^{-1} observed at the early epochs ($\sim$30 days before maximum) was unusually low compared with typical Type Ib SNe (Branch et al. 2002).

The unique properties of SN 2005bf summarized above indicate an unusual event, one having certain features in common with ordinary Type Ib/c SNe (see § 4.1), Type IIb events like SN 1993J (Filippenko et al. 1993), and highly energetic supernovae like those seen in conjunction with GRBs 990425 (Galama et al. 1998) and 030329 (Hjorth et al. 2003). Both the high luminosity at the main peak and the long rise time argue for a more massive helium core and larger mass of ^{56}Ni than ordinary Type Ib/Ic SNe. Assuming a light curve dominated at peak by radioactive decay and complete trapping, to produce a luminosity of 6×10^{42} erg s^{-1} 40 days after the explosion requires about 0.6 M$_\odot$ of ^{56}Co (made as ^{56}Ni in the explosion). Such a large mass of ^{56}Ni is not produced in spherically symmetric explosions unless the explosion energy is very high, much greater than the canonical 10^{51} erg, and the density gradient near the iron core, shallow, as in massive stars ($\gtrsim$25 M$_\odot$) (Woosley & Weaver 1995).

On the other hand, the comparative faintness of the light curve during its first few days and the fact that the effective temperature was *increasing* at earlier times, rather than cooling, argue for a compact progenitor, neither a red nor blue supergiant. A red supergiant of any sort would be too bright and too hot initially and would cool monotonically. A blue supergiant with a radioactive peak around 40 days would be too faint on day 10 and would also have a declining temperature at early times.

The high velocity hydrogen (with no low velocity counterpart) shows that the star had lost most, but not all of its hydrogen envelope. The surface layers are shock accelerated to the highest speeds and a low mass of hydrogen would not mix extensively with the rest of the star. It seems that the progenitor was a Wolf-Rayet star of spectral class WN (Maeder & Meynet 1994) with less than 0.1 $M_{\odot}$ of hydrogen in its outer layers.

Within these confines, we explored a variety of models, but found no physically reasonable solutions under the assumption of spherical symmetry and a monotonically decreasing radial abundance of ^{56}Ni. The most successful 1D model was the 2.0×10^{51} erg explosion of an 8.29 $M_{\odot}$ WN star with a mildly *inverted* distribution of ^{56}Ni with mass as shown in Figure 9. This star had a total ^{56}Ni mass of 0.6 $M_{\odot}$, of which about 0.04 $M_{\odot}$ was artificially sited in the helium shell. Except for the unusual "mixing", this was essentially the same helium and heavy element core one obtains by evolving a 25 $M_{\odot}$ main sequence star to its end point. The vast bulk of the hydrogenic envelope was presumably lost to a binary companion quite late in the evolution. We did not conduct a broad survey of progenitor masses because we thought the restriction of doing 1D models did not warrant such an approach. It is possible that an acceptable model might also have been found for a higher mass helium core and larger explosion energy. Roughly the outer 0.05 $M_{\odot}$ of this WN star was composed of hydrogen and helium with mass fractions of 0.34 and 0.66, respectively. Terminal velocities ranged from 13,000 km s^{-1} at the base of this "envelope" to over 30,000 km s^{-1} in the outer 0.001 $M_{\odot}$. The rms velocity in the hydrogen rich material was 18,000 km s^{-1}. All calculations of presupernova evolution and explosive hydrodynamics up to the point of shock outbreak were calculated using the KEPLER implicit hydrodynamics package (Weaver, Zimmerman, & Woosley 1978; Woosley et al. 2002). The hydrogen envelope was removed at the end of helium burning and the star was in hydrostatic and thermal equilibrium at the time it exploded.

The light curve and multi-band photometry of this model were then calculated using the STELLA code of Blinnikov et al. (1998) and Blinnikov & Sorokina (2000). Though no fine tuning was attempted, Figure 10 shows that this model gave a qualitatively good fit to both the observed bolometric luminosity and individual colors up until the main peak. To achieve reasonable agreement beyond the main peak however, much greater gamma-ray leakage had to be invoked than was calculated by STELLA for the spherically symmetric model. This was achieved by turning down the gamma-ray opacity by a factor of 10 while leaving the UVOIR opacities unaltered. During the rise to maximum this alteration had no effect since the optical depth was very large. After the maximum though, the decline rate was greatly accelerated. We were unable to find a model with unaltered gamma-ray opacity in which the light curve peaked so late and yet declined so quickly.

All of these characteristics — the high explosion energy, large ^{56}Ni mass, inverted distribution of ^{56}Ni, and the need for γ-ray leakage at late times — are suggestive of a grossly asymmetric explosion having many features in common with the supernovae found coincident with GRBs (e.g. Höflich, Wheeler, & Wang 1999; Mazzali et al. 2001; Maeda et al. 2003; Mazzali et al. 2005). In fact, SN 2005bf may be the best example so far of a transition object between the two classes of phenomena, namely GRBs and ordinary Type Ib SNe. A realistic simulation of such event will only be achievable in a multi-dimensional simulation that captures the essence of energetic polar jets with milder mass ejection in the equatorial plane. Lacking the present ability to do such a full multi-dimensional, relativistic simulation including the necessary radiation transport, we also considered multi-component models to reproduce the observed light curves. The scenario we considered was that of a WN progenitor star of about 6 to 15 solar masses whose iron core collapses either to a black hole plus an accretion disk (Woosley 1993; MacFadyen & Woosley 1999) or a very rapidly rotating neutron star (Wheeler et al. 2000). A relativistic jet was launched, as in current models for GRBs, but it was not observed, possibly because it was beamed to other angles or because it had too little energy in extremely relativistic ejecta. The jet was accompanied, however, by vigorous ^{56}Ni-rich outflows extending out to approximately 45 degrees (MacFadyen & Woosley 1999).

The polar regions thus experienced a much more violent explosion than the equator. A small fraction of the star's mass was ejected with very high velocity at both poles along the star's rotational axis. This material contained about 0.1 $M_\odot$ of ^{56}Ni per pole and the observer was situated somewhat off axis. The ensuing explosion can be separated into two components: 1) a polar explosion containing a small fraction of the total mass and moving at high velocity, and 2) the explosion of the rest of the star. At first only the polar explosion is observed, producing the initial maximum, and only when that component fades and becomes transparent, does the lower velocity ejecta become visible in the rise to the main maximum light.

As a specific example, by no means unique, we consider the same 8.29 $M_\odot$ WN star as before, but with no mixing of the ^{56}Ni beyond where it was produced in the 1D model (the dashed line in Figure 9). In addition to this, we represent the higher velocity component by the 2×10^{51} erg explosion of a 3.31 $M_\odot$ WR star that left behind a 1.52 $M_\odot$ remnant (hence the 2×10^{51} erg is concentrated in 1.79 $M_\odot$ of ejecta). This component contains 0.1 $M_\odot$ of ^{56}Ni (presumably at each pole). The composite light curve and colors are given in Figure 11. At early times ($t < 20$ days), before the fast expanding, low mass component has become optically thin, the slower moving explosion is occulted and blocked from view. At late times ($t > 20$ days), the fast moving component is invisible. The geometry of the slower moving ejecta resembles the number "8" viewed from its side. Gamma-rays can diffuse out much more effectively along the polar axis than the equator. To account for this, the gamma-ray opacity has been reduced by a factor of 10.

6. CONCLUSIONS

The computer simulations presented here, though clearly suffering from being one-dimensional, strongly suggest that the light curve and the two component spectrum can be qualitatively explained by the very energetic explosion of a massive star that lost almost all of its hydrogen envelope and exploded very asymmetrically. The energy and ^{56}Ni mass implied are large compared with common Type Ib SNe, but the energy is intermediate between ordinary supernovae and "hypernovae", suggesting SN 2005bf might be some sort of transition object between these two classes of phenomena. Given the high energy, and the possible detection of polarization (Wang & Baade 2005), it is very likely that the explosion was asymmetric and will ultimately need to be modeled in at least two dimensions. The ^{56}Ni distribution could have been very aspherical and that particularly complicates the modeling of the first peak.

Given the previously observed association of GRBs and energetic supernovae, it is quite plausible that SN 2005bf was powered by a central engine like those being discussed for GRBs. To retain the necessary degree of rotation, it is more likely that the envelope of the star was lost to a binary companion rather than an ordinary standard wind. The longer the star remains a red supergiant, the more its core is braked by torques from the slowly rotating envelope (Heger, Woosley, & Spruit 2005; Woosley & Heger 2005). Two-dimensional simulations are encouraged to verify the interpretation of this event as a possible "missing link". Radio observations to limit the amount of relativistic ejecta are also encouraged.

We would like to thank David Branch for allowing us to use SYNOW, and Jerod Parrent for providing us with the code. This material is based upon work supported by the National Science Foundation under Grant No. 0306969. We also acknowledge support from the HST grant GO-09860.07-A. MH acknowledges support provided by NASA through Hubble Fellowship grant HST-HF-01139.01-A awarded by the Space Telescope Science Institute, which is operated by the Association of Universities for Research in Astronomy, Inc., for NASA, under contract NAS 5-26555. MH and GG thank support from the Centro de Astrofísica FONDAP 15010003. BLL was supported by an NSERC PGS B and a Walter C. Sumner Fellowship.

REFERENCES

Bessell, M. S. 1999, PASP, 111, 1426

Blinnikov, S. I., Eastman, R., Bartunov, O.S., Popolitov, V.A., & Woosley, S.E., 1998, ApJ, 496, 454

Blinnikov, S.I., & Sorokina, E.I. 2000, A&A, 356, L30.

Branch, D., et al. 2002, ApJ, 566, 1005

Cardelli, J. A., Clayton, G. C., & Mathis, J .S. 1989, ApJ, 345, 245

Clocchiatti, A., & Wheeler, J. C. 1997, ApJ, 491, 375

Fisher, A. 2000, Ph.D. thesis, Univ. Oklahoma

Falco, E. E., et al. 1999, PASP, 111, 438

Filippenko, A. V., Matheson, T., & Ho, L. C. 1993, ApJ, 415, L103

Filippenko, A. V., et al. 1995, ApJ, 450, L11

Freedman, W. L., et al. 2001, ApJ, 553, 47

Fukugita, M., Ichikawa, T., Gunn, J. E., Doi, M., Shimasaku, K., Schneider, D. P. 1996, AJ, 111, 1748

Galama, T. J., et al. 1998, Nature, 395, 670

Hamuy, M., Suntzeff, N. B., Heathcote, S. R., Walker, A. R., Gigoux, P., Phillips, M. M. 1994, PASP, 106, 566

Hamuy, M., et al. 2002, AJ, 124, 417

Hamuy, M. 2004, in Stellar Collapse, ed. C. L. Fryer (Dordrecht:Kluwer), 39

Hamuy, M., Contreras, C., Gonzalez, S., & Krzeminski, W. 2005a, IAU Circ., 8520

Hamuy, M., et al. 2005b, PASP, in preparation (**Paper I**)

Harkness, R. P., et al. 1987, ApJ, 317, 355

Heger, A., Woosley, S. E., & Spruit, H. C. 2005, ApJ, 626, 350

Hjorth, J., et al. 2003, Nature, 423, 847

Höflich, P., Wheeler, J. C., & Wang, L. 1999, ApJ, 521, 179

Iwamoto, K., et al. 2000, ApJ, 534, 660

MacFadyen, A. I., & Woosley, S. E. 1999, ApJ, 524, 262

Maeda, K., Mazzali, P. A., Deng, J., Nomoto, K., Yoshii, Y., Tomita, H., & Kobayashi, Y. 2003, ApJ, 593, 931

Maeder, A., & Meynet, G. 1994, A&A, 287, 803

Mazzali, P. A., Nomoto, K., Patat, F., & Maeda, K. 2001, ApJ, 559, 1047

Mazzali, P. A., et al. 2005, Science, 308, 1284

Modjaz, M., Kirshner, R., & Challis, P. 2005, IAU Circ., 8509

Monard, L. A. G., Moore, M., & Li, W. 2005, IAU Circ., 8507

Morrell, N., Hamuy, M., Folatelli, G, & Contreras, C. 2005, IAU Circ., 8509

Panagia, N. 2003, in Lecture Notes in Physics, 598, Supernovae and Gamma Ray Bursters, ed. K. W. Weiler (Berlin: Springer), 113

Patat, F. et al. 2001, ApJ, 555, 900

Richmond, M. W., et al. 1994, AJ, 107, 1022

Schlegel, E. M. 1990, MNRAS, 244, 269

Schlegel, D. J., Finkbeiner, D. P., & Davis, M. 1998, ApJ, 500, 525

Smith, J. A., et al. 2002, AJ, 123, 2121

Stanek, K. Z., et al. 2005, ApJ, 626, L5

Stritzinger, M., et al. 2002, AJ, 124, 2100

Turatto, M., Benetti, S., & Cappellaro, E. 2003, in ESO/MPA/MPE Workshop (an ESO Astrophysics Symp.), From Twilight to Highlight: the Physics of Supernovae, ed. B. Leibundgut, & W. Hillebrandt (Berlin: Springer-Verlag), 200

Wang, L., & Baade, D. 2005, IAU Circ., 8521

Weaver, T. A., Zimmerman, G. B., & Woosley, S. E. 1978, ApJ, 225, 1021

Wheeler, J. C., Harkness, R.P., Clocchiatti, A., Benetti, S., Brotherton, M. S., DePoy, E. L., & Elias, J. 1994, ApJ, 436, L135

Wheeler, J. C., Yi, I., Höflich, P., & Wang, L. 2000, ApJ, 537, 810

Woosley, S. E. 1988, ApJ, 330, 218

Woosley, S. E. 1993, ApJ, 405, 273

Woosley, S. E., & Weaver, T. A. 1995, ApJS, 101, 181

Woosley, S. E., Heger, A., & Weaver, T. A. 2002, Reviews of Modern Physics, 74, 1015

Woosley, S. E., & Heger, A. 2005, submitted to ApJ, astroph-0508175

This preprint was prepared with the AAS LaTeX macros v5.2.

Table 1. Photometry of the comparison stars in the field of SN 2005bf

Star ID	u'	g'	r'	i'	B	V
C1	···	···	···	···	14.657(016)	···
C2	16.360(021)	15.186(015)	14.762(015)	14.630(015)	15.545(009)	14.943(010)
C3	19.203(016)	16.529(008)	15.463(009)	15.067(009)	17.141(009)	15.963(008)
C4	17.105(016)	···	···	···	15.081(016)	···
C5	19.988(034)	17.292(009)	16.115(008)	15.624(008)	17.938(010)	16.675(007)
C6	16.254(020)	15.147(011)	14.753(011)	14.603(011)	15.476(009)	14.905(010)
C7	21.254(205)	18.924(009)	18.013(008)	17.676(008)	19.446(016)	18.434(008)
C8	18.328(013)	17.040(008)	16.529(008)	16.328(008)	17.433(009)	16.743(007)
C9	22.883(797)	20.755(028)	19.362(018)	18.302(009)	19.504(477)	19.957(024)
C10	19.416(033)	18.473(009)	18.125(008)	18.022(013)	18.770(011)	18.259(008)
C11	20.418(046)	18.628(008)	17.953(008)	17.691(008)	19.104(015)	18.247(008)
C12	19.604(044)	17.845(008)	17.176(008)	16.939(008)	18.326(015)	17.472(007)
C13	21.969(371)	20.692(053)	19.294(017)	17.730(010)	21.872(192)	19.940(029)
C14	17.251(019)	15.996(008)	15.520(008)	15.353(008)	16.371(009)	15.709(007)

Note. — Uncertainties given in parentheses in thousandths of a magnitude correspond the an rms of the magnitudes obtained on four photometric nights, with a minimum uncertainty of 0.015 mag for an individual measurement.

Table 2. $u'g'r'i'BV$ Photometry for SN 2005bf

JD $-2,453,000$	Epoch[a] (days)	Telescope	u'	g'	r'	i'	B	V	T_{bb} (K)	$\log L_{(u' \to i')}$ (erg s^{-1})	$\log L_{\rm bol}$ (erg s^{-1})
444.81	−54	KAIT	···	···	> 20.0	···	···	···	···	···	···
459.79	−39	KAIT	···	···	19.441(197)	···	···	···	···	···	(41.544)
466.80	−32	KAIT	···	···	18.070(062)	···	···	···	···	···	(42.100)
467.65	−32	Swope	18.691(021)	17.991(015)	17.935(015)	18.048(015)	18.191(016)	17.962(015)	9567	42.014	42.146
468.58	−31	Swope	18.436(016)	17.891(015)	17.881(015)	18.006(017)	18.086(016)	17.894(015)	10082	42.061	42.183
472.59	−27	Swope	17.983(016)	17.571(015)	17.575(015)	17.659(015)	17.750(016)	17.581(015)	10040	42.203	42.325
473.61	−26	Swope	17.908(016)	17.508(015)	17.513(015)	17.582(015)	17.701(016)	17.520(015)	9872	42.228	42.352
474.57	−25	Swope	17.939(016)	17.478(015)	17.462(015)	17.526(015)	17.686(016)	17.464(015)	9575	42.236	42.365
475.64	−24	Swope	17.994(016)	17.484(015)	17.409(015)	17.481(015)	17.678(016)	17.451(015)	9214	42.237	42.373
475.78	−24	KAIT	···	···	17.419(062)	···	···	···	···	···	···
476.56	−23	Swope	18.092(016)	17.510(015)	17.406(015)	17.477(015)	17.721(016)	17.460(015)	8912	42.223	42.365
476.73	−23	KAIT	···	···	17.426(033)	···	···	···	···	···	···
477.56	−22	Swope	18.244(016)	17.543(015)	17.371(015)	17.414(015)	17.762(016)	17.475(015)	8297	42.209	42.366
478.57	−21	Swope	18.348(017)	17.554(015)	17.344(015)	17.392(015)	17.806(016)	17.457(015)	7974	42.200	42.366
479.52	−20	Swope	18.443(023)	17.550(015)	17.298(015)	17.328(015)	17.792(016)	17.397(015)	7713	42.206	42.381
480.54	−19	Swope	18.554(020)	17.524(015)	17.275(015)	17.294(015)	17.787(016)	17.365(015)	7622	42.206	42.387
481.51	−18	Swope	18.587(026)	17.496(015)	17.208(015)	17.253(015)	17.777(016)	17.346(015)	7462	42.215	42.400
482.52	−17	Swope	18.583(050)	17.462(030)	17.134(026)	17.150(020)	17.715(025)	17.282(022)	7262	42.238	42.433
483.54	−16	Swope	18.530(037)	17.370(015)	17.113(015)	17.148(015)	17.646(016)	17.223(015)	7596	42.258	42.442
484.61	−15	Swope	18.369(041)	17.314(015)	17.060(015)	17.082(015)	17.616(016)	17.166(015)	7485	42.285	42.469
489.51	−10	Swope	17.871(016)	16.905(015)	16.704(015)	16.746(015)	17.148(016)	16.808(015)	8033	42.448	42.617
490.50	−9	Swope	17.681(016)	16.787(015)	16.622(015)	16.688(015)	17.029(016)	16.722(015)	8350	42.493	42.652
491.48	−8	Swope	17.506(016)	16.694(015)	16.552(015)	16.645(017)	16.923(016)	16.630(015)	8675	42.534	42.683
493.51	−6	Swope	17.273(043)	16.603(015)	···	···	16.799(025)	16.532(015)	8677	42.586	42.734
495.53	−4	Swope	17.147(016)	16.528(015)	···	···	16.754(016)	16.477(015)	8486	42.616	42.768
496.54	−3	Swope	17.145(017)	16.501(015)	···	···	16.724(016)	16.472(015)	8449	42.624	42.778
497.46	−2	Swope	17.097(016)	16.493(015)	···	···	16.697(016)	16.448(015)	8333	42.635	42.793
497.47	−2	Clay	···	···	16.348(015)	16.347(030)[b]	···	···	···	···	···
499.45	0	Swope	17.105(016)	16.495(015)	···	···	16.730(016)	16.432(015)	8051	42.636	42.799
500.46	1	Swope	17.142(016)	16.529(015)	···	···	16.743(016)	16.460(015)	7873	42.628	42.798
501.46	2	Swope	17.198(016)	16.559(015)	···	···	16.801(016)	16.460(015)	7601	42.617	42.794
502.46	3	Swope	17.261(016)	16.586(015)	···	···	16.829(016)	16.483(015)	7466	42.607	42.789
503.46	4	Swope	17.346(016)	16.619(015)	···	···	16.875(016)	16.502(015)	7298	42.592	42.781
504.48	5	Swope	17.418(016)	16.653(015)	···	···	16.928(016)	16.518(015)	7141	42.578	42.773

Table 2—Continued

JD $-2,453,000$	Epoch[a] (days)	Telescope	u'	g'	r'	i'	B	V	T_{bb} (K)	$\log L_{(u' \to i')}$ (erg s^{-1})	$\log L_{\rm bol}$ (erg s^{-1})
506.47	7	Swope	17.620(016)	16.749(015)	···	···	17.055(016)	16.571(015)	6798	42.540	42.751
508.65	9	Swope	···	···	16.489(015)	16.393(015)	17.182(016)	16.636(015)	6592	42.497	42.720
509.46	9	Swope	···	···	16.474(015)	16.397(015)	17.250(016)	16.664(015)	6371	42.484	42.716
510.50	11	Swope	···	···	16.501(015)	16.418(015)	17.317(023)	16.706(017)	6225	42.462	42.703
511.48	11	Swope	···	···	16.550(015)	16.447(015)	17.423(016)	16.766(015)	6048	42.434	42.687
512.65	13	Swope	18.313(062)	17.123(015)	16.579(015)	16.441(015)	17.561(018)	16.835(015)	5719	42.404	42.682
513.46	13	Swope	···	···	16.626(015)	16.490(015)	17.570(016)	16.881(015)	5776	42.387	42.662
516.45	16	Swope	18.695(024)	17.426(015)	···	···	17.863(016)	17.052(015)	5383	42.304	42.614
517.45	17	Swope	18.792(071)	17.513(029)	···	···	17.992(016)	17.127(015)	5240	42.273	42.596
520.46	20	Swope	19.271(035)	17.801(015)	···	···	18.324(016)	17.367(015)	4945	42.169	42.529
521.44	21	Swope	19.361(043)	17.854(022)	···	···	18.399(016)	17.439(015)	4938	42.141	42.504
522.45	22	Swope	···	···	17.195(015)	16.924(015)	18.478(025)	17.535(018)	4879	42.109	42.480
523.47	23	Swope	···	···	17.263(015)	17.018(015)	18.609(018)	17.641(015)	4821	42.070	42.446
524.45	24	Swope	···	···	17.377(020)	17.075(027)	18.737(017)	17.697(015)	4750	42.034	42.423
525.45	25	Swope	···	···	17.421(015)	17.127(015)	18.811(038)	17.773(027)	4698	42.007	42.403
526.45	26	Swope	···	···	17.458(015)	17.201(015)	18.975(051)	17.878(018)	4575	41.974	42.381
527.51	27	Swope	···	···	17.540(015)	17.313(015)	18.987(016)	17.953(015)	4688	41.942	42.333
528.47	28	Swope	···	···	···	···	18.999(016)	18.003(015)	4737	41.920	42.305
529.48	29	Swope	20.260(046)	18.535(015)	···	···	19.097(017)	18.061(015)	4713	41.891	42.275
530.47	30	Swope	20.274(039)	18.588(021)	···	···	19.167(018)	18.105(017)	4729	41.870	42.245
538.48	38	Swope	···	···	···	···	19.520(037)	18.464(015)	···	···	(42.124)
538.49	38	Swope	···	···	···	···	19.583(043)	18.472(015)	···	···	(42.135)
539.46	39	Swope	···	···	···	···	···	18.484(019)	···	···	···
542.46	42	Swope	···	···	···	···	19.776(068)	18.598(018)	···	···	(42.103)
565.47	64	Swope	···	···	19.061(416)	18.715(177)	20.403(063)	19.357(022)	4685	41.279	41.734
569.47	68	Swope	···	···	···	···	20.625(133)	19.582(042)	···	···	(41.673)

Note. — Photometry uncertainties given in parentheses in thousandths of a magnitude. A minimum uncertainty of 0.015 mag was set.

[a]Rest-frame days since $L_{\rm bol}$ maximum (JD 2,453,499.8).

[b]Synthetic magnitude computed from the spectrum obtained the same night.

Table 3. Light Curve Parameters for SN 2005bf

Filter	JD at Peak $-2,453,000$	Peak Magnitude
u'	497.9 ± 0.5	17.10 ± 0.01
g'	498.1 ± 0.5	16.50 ± 0.01
r'	500.2 ± 1.0	16.32 ± 0.01
i'	502.9 ± 1.0	16.32 ± 0.02
B	497.4 ± 0.5	16.71 ± 0.02
V	498.8 ± 0.5	16.44 ± 0.01
M_{bol}	499.8 ± 0.5	−18.32 ± 0.03[a]

Note. — Uncertainties in the peak magnitudes were estimated from the rms of the photometric points about a low-order polynomial fit. Uncertainties in the dates of maximum are based on the data sampling rates.

[a]Absolute bolometric magnitude based on L_{bol} from Table 2 (no host-galaxy extinction correction applied).

Table 4. Near-infrared photometry of two comparison stars

Star ID	Y	J	H	K_s
C10	17.40(02)	17.16(02)	16.87(05)	16.72(06)
C11	16.97(02)	16.58(02)	16.12(02)	16.00(03)

Note. — Uncertainties given in parentheses in hundredths of a magnitude. A minumum uncertainty of 0.02 mag was set.

Table 5. Near-Infrared Photometry for SN 2005bf

JD $-2,453,000$	Epoch[a] (days)	Y	J	H	K_s	Instrument
483.51	−16	16.93(02)	16.75(02)	16.65(02)	···	WIRC
483.52	−16	16.92(02)	16.76(02)	16.64(02)	···	WIRC
511.46	11	16.19(02)	15.95(02)	15.87(02)	15.80(03)	PANIC
538.46	38	···	16.91(02)	···	16.43(02)	PANIC

Note. — WIRC data were obtained with two detectors and their magnitudes agree within uncertainties. We used the averages in the present analysis. Uncertainties are given in parentheses in hundredths of a magnitude. A minumum uncertainty of 0.02 mag was set.

[a]Rest-frame days since $L_{\rm bol}$ maximum (JD 2,453,499.8).

Table 6. Spectroscopic observations of SN 2005bf

JD $-2,453,000$	Epoch[a] (days)	Instrument	Wavelength Range (Å)	Resolution[b] (Å)	Exposure (s)	$\langle S/N \rangle$[c] (in 10 Å)
467.57	-32	WFCCD	3800 – 9235	8	900	69
472.60	-27	WFCCD	3800 – 9235	8	900	88
475.63	-24	WFCCD	3800 – 9235	8	900	74
479.51	-20	WFCCD	3800 – 9235	8	700	32
497.47	-2	LDSS-3	3838 – 10000	4[d]	200	262
502.48	3	LDSS-3	6057 – 10000	5	900	200
521.50	21	WFCCD	3800 – 8125	8[e]	1200	64
523.49	23	WFCCD	3800 – 8128	8	1200	42
527.54	27	WFCCD	3800 – 8128	8	600	55

Note. — Some spectra are the combination of multiple observations. In those cases, total exposure times are given.

[a]Rest-frame days since $L_{\rm bol}$ maximum (JD 2,453,499.8).

[b]Average resolution obtained from the FWHM of arc-lamp lines.

[c]Average signal-to-noise ratio in 10 Å bins calculated in the range from 4000 to 8000 Å.

[d]Resolution of 2.9 Å in the blue channel ($3800 < \lambda < 6000$ Å), and 4.7 Å in the red channel ($6000 < \lambda < 10000$ Å).

[e]A wide slit ($8.''65$) was used. In this case the resolution was estimated from the FWHM of the spatial profile of the SN.

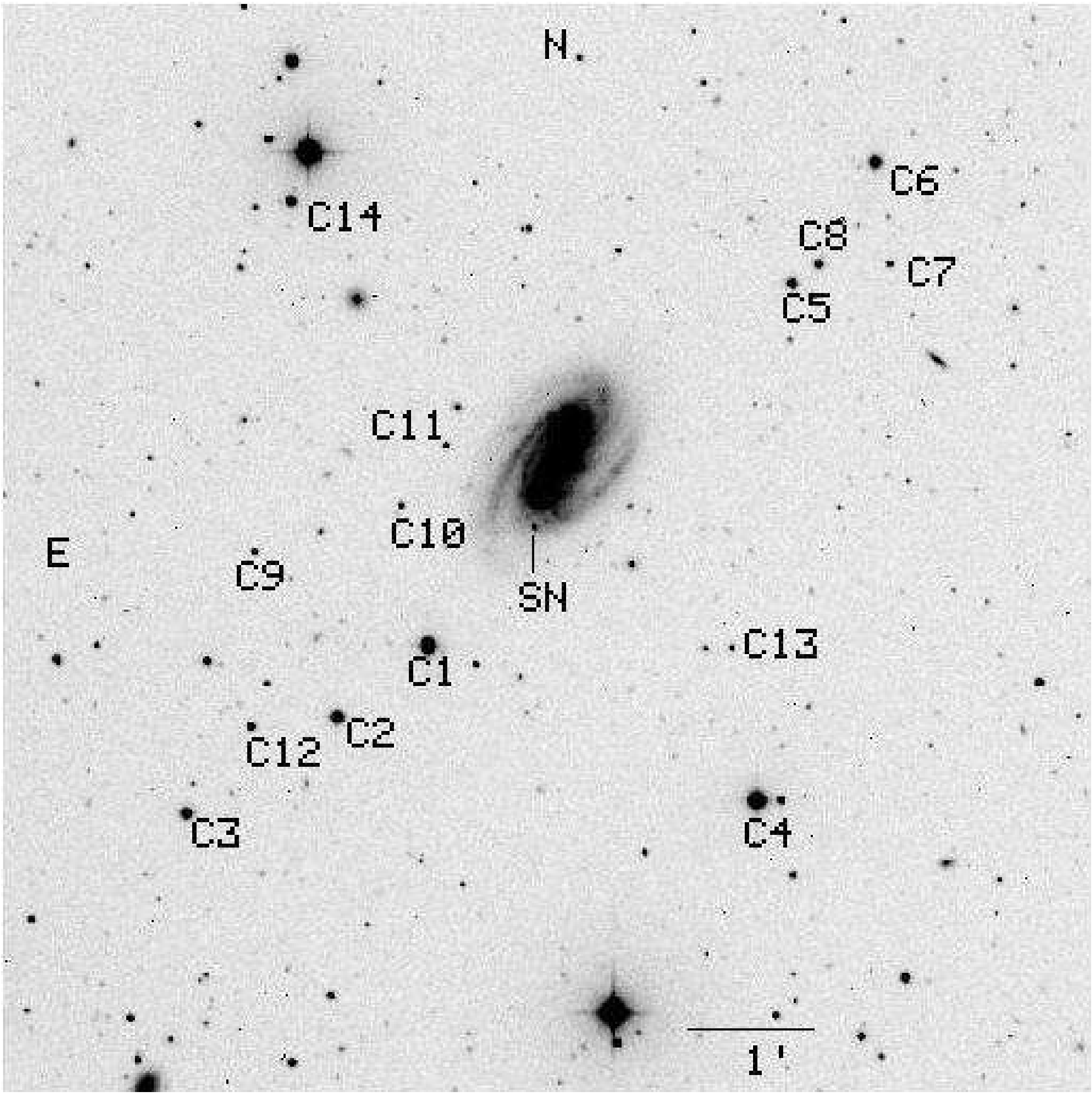

Fig. 1.— The field of SN 2005bf observed with the Swope 1-m telescope at LCO and a V filter. North is up and East is to the left. The supernova is marked to the SE of the host galaxy nucleus. Fourteen comparison stars used to derive differential photometry of the SN are labeled. The plate scale is shown near the bottom.

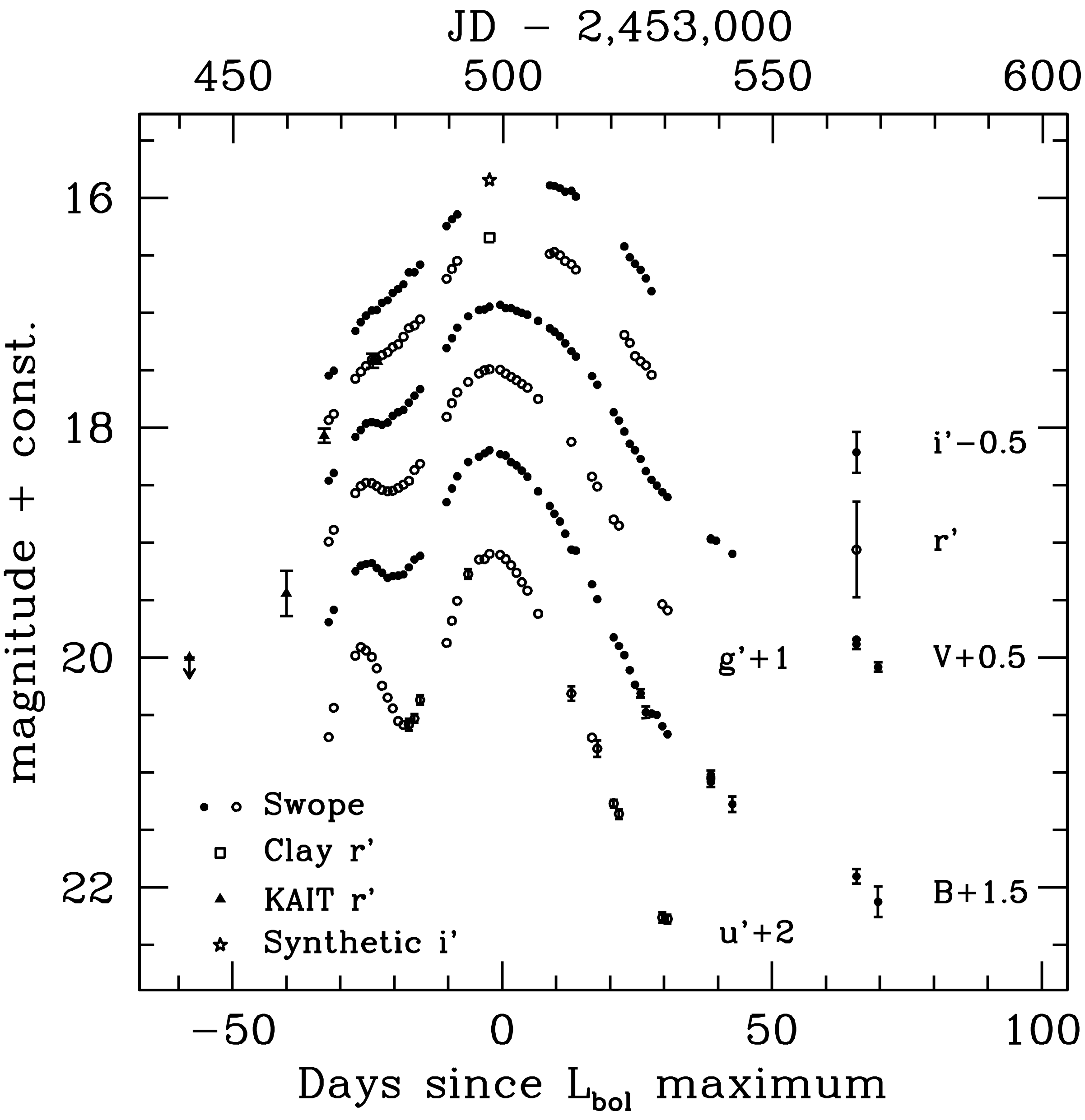

Fig. 2.— Observed $u'g'r'i'BV$ light curves of SN 2005bf from Swope (*open and closed circles*), KAIT (*closed triangles*), and Clay (*open square*). A star symbol marks a synthetic i' magnitude obtained from the LDSS-3 spectrum of May 7 (∼JD 2,453,497). The arrow marks an r' lower limit from a KAIT image obtained on March 15 (∼JD 2,453,445). Unless explicitly drawn, the error bars are smaller than the symbols. The time axes are given in the observer's frame. For clarity, the magnitudes in each band have been shifted by an arbitrary constant.

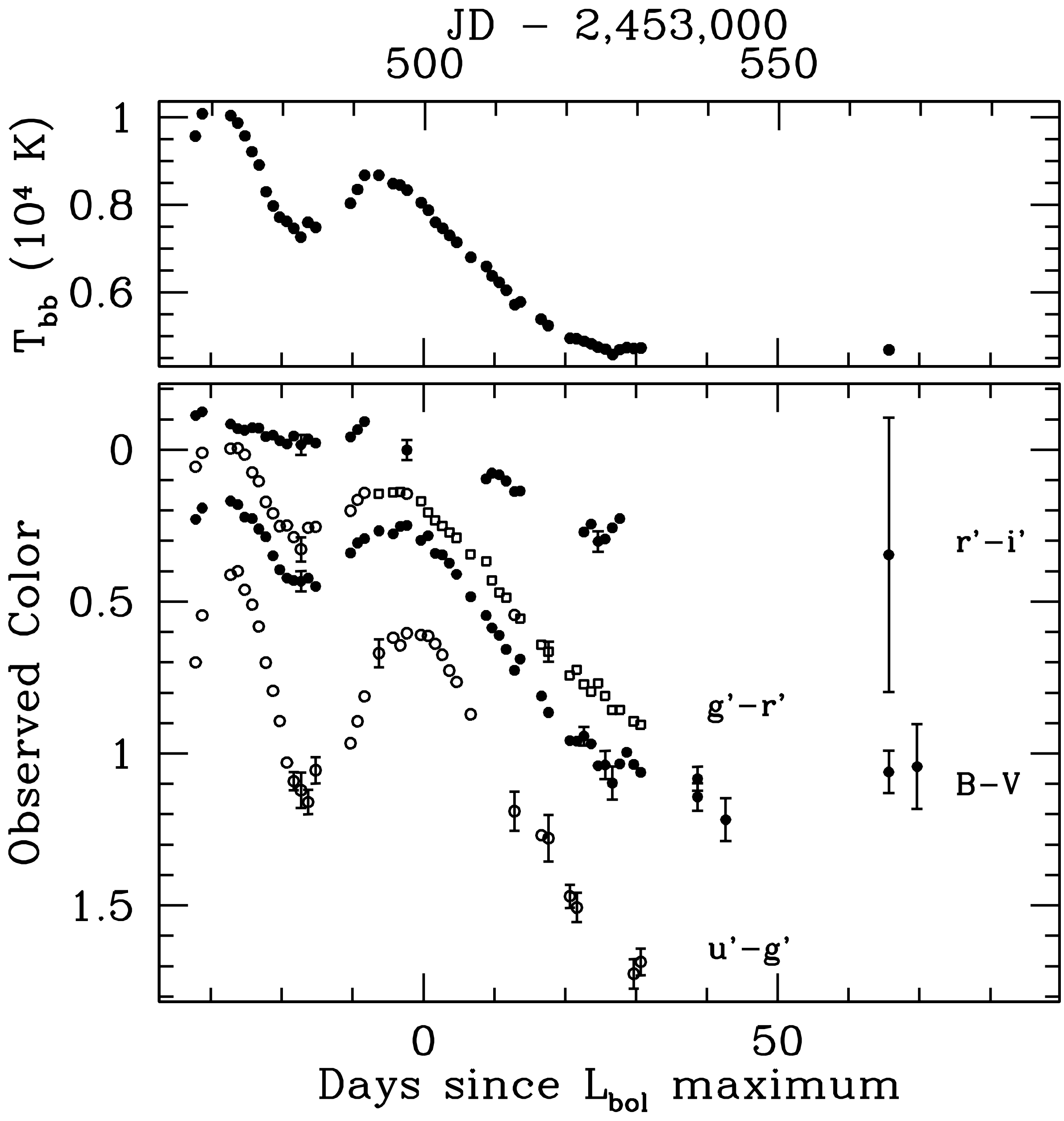

Fig. 3.— (top) Temperature T_{bb} from the blackbody fits to the B through i' monochromatic fluxes. (bottom) Observed color evolution for $(u' - g')$, $(B - V)$, $(g' - r')$, and $(r' - i')$. Circles mark colors computed directly from measurements in both bands while squares are used when one of the lightcurves was interpolated in time. Unless explicitly drawn, the error bars are smaller than the symbols. The time axes are given in the observer's frame. No reddening correction was applied.

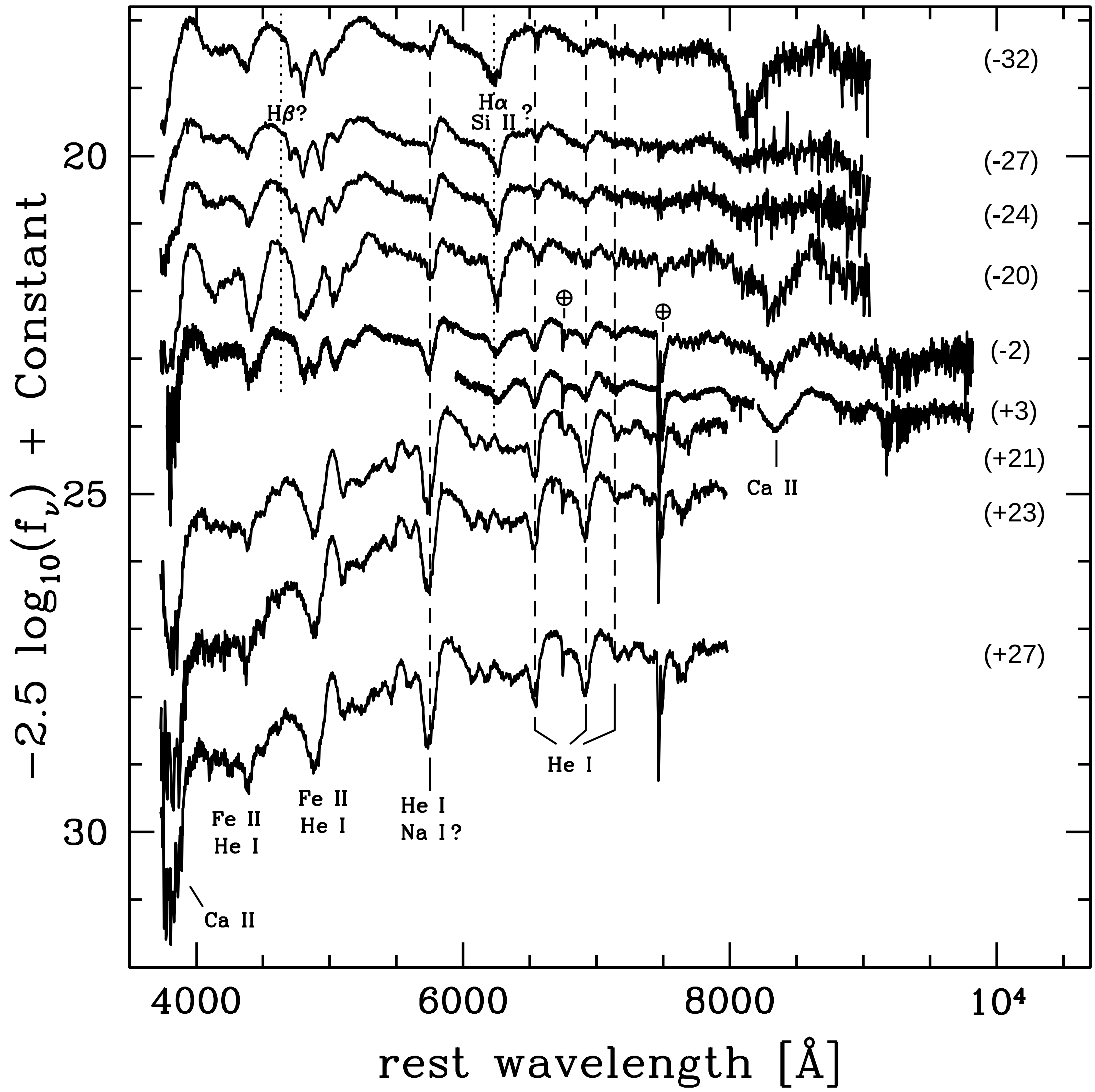

Fig. 4.— Spectroscopic evolution of SN 2005bf. Each spectrum is presented in logarithmic scale, shifted by an arbitrary constant. The wavelength of the spectra was shifted to the SN rest frame using a redshift of z = 0.01833. The labels in parentheses to the right of each spectrum indicate the epoch in rest-frame days since $L_{\rm bol}$ maximum (JD = 2,453,499.8). The spectrum from day −20 was smoothed by averaging in five dispersion elements. The name of the ions responsible for some of the main features are given. The dotted vertical lines mark the wavelength at which the minimum of the Hα and Hβ lines would appear if hydrogen was present at $\sim$14,500 km s^{-1}. The dashed vertical lines mark the absorptions due to He I $\lambda\lambda$ 5876,6678,7065,7281, at an expansion velocity of $\sim$6,000 km s^{-1}. Telluric features are marked with an Earth symbol ($\oplus$).

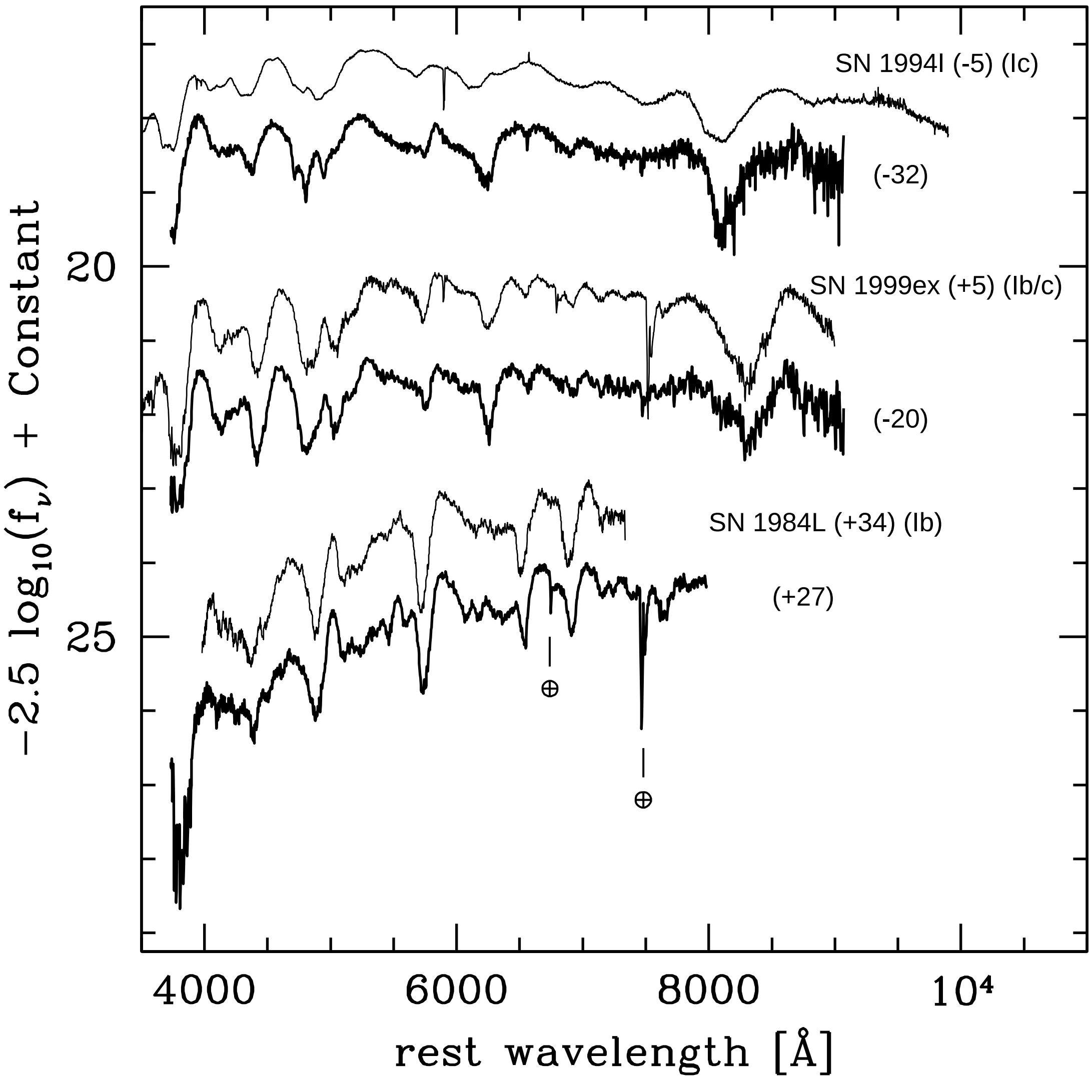

Fig. 5.— Comparison of spectra of SN 2005bf with those of other Type Ib and Type Ic SNe. At the top, the spectrum from day −32 compared with that of the Type Ic SN 1994I five days before maximum light (Filippenko et al. 1995). At the middle, the spectrum from day −20 and that of the Type Ib/Ic SN 1999ex five days after maximum light (Hamuy et al. 2002). At the bottom, the spectrum from day +27 and that of the Type Ib SN 1984L 34 days after maximum light (Harkness et al. 1987). Telluric features are marked with an Earth symbol (⊕).

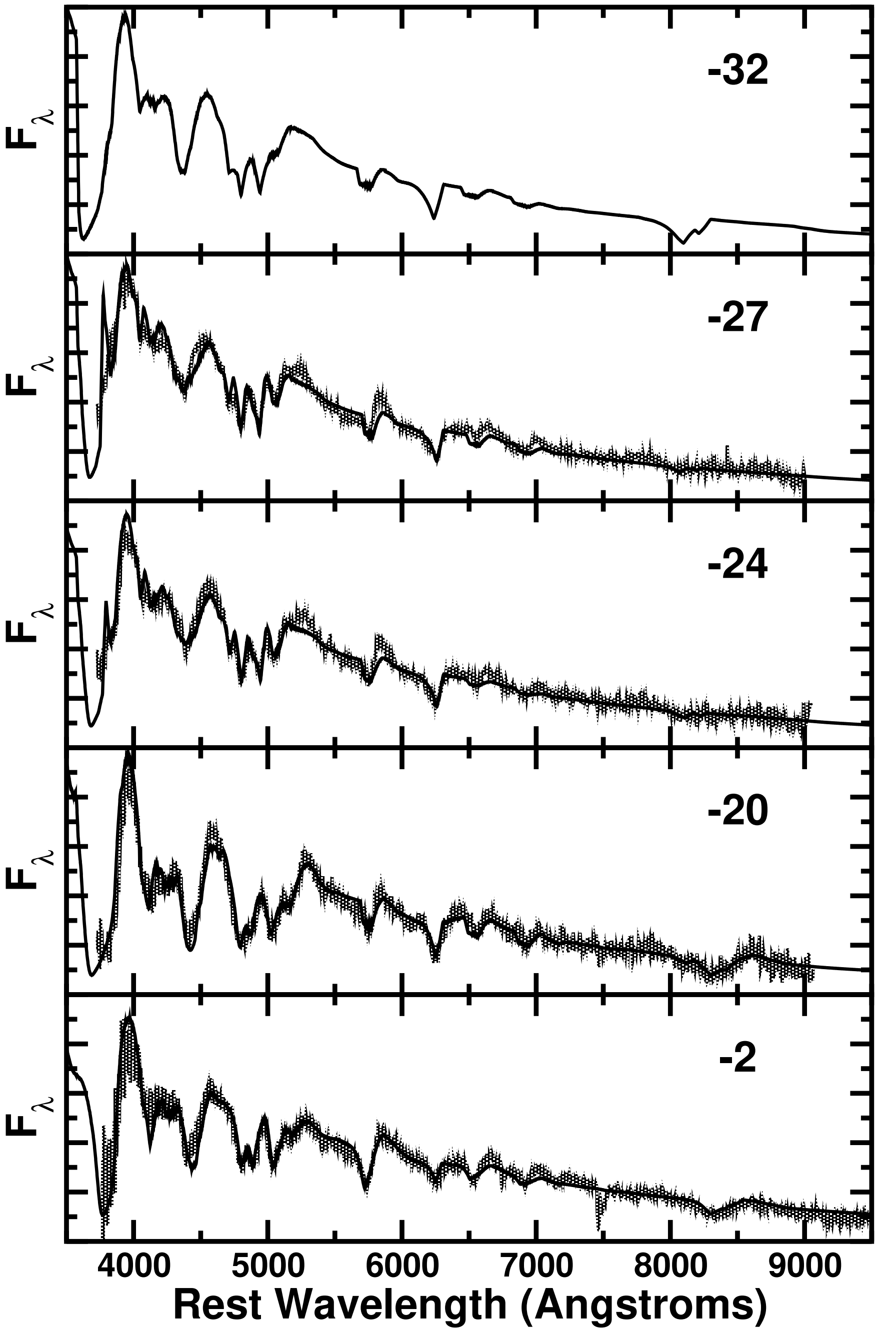

Fig. 6.— SYNOW synthetic spectra fits to the pre-maximum spectra of SN 2005bf. The synthetic spectra, which are described in the text, are overplotted on the observed spectra.

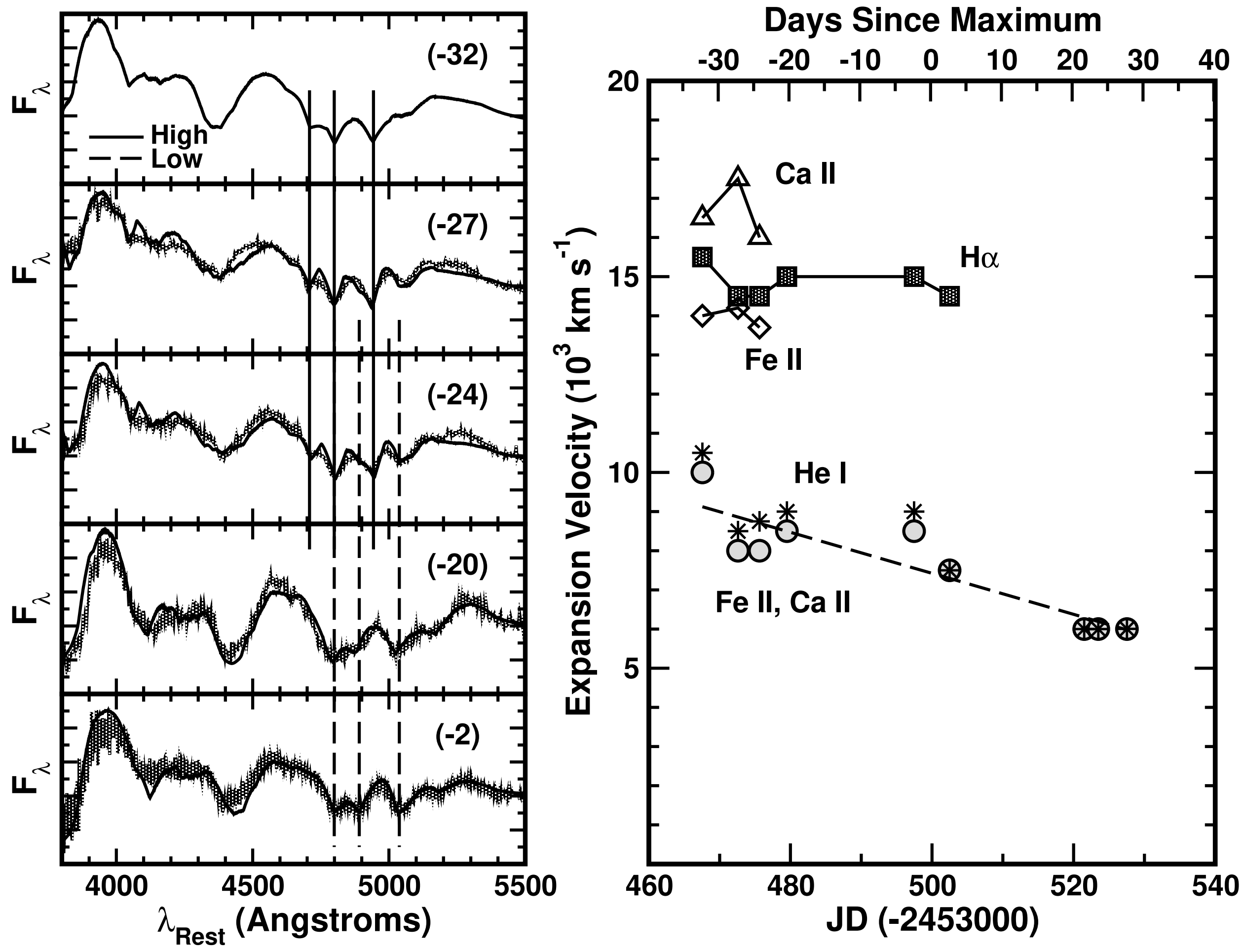

Fig. 7.— (left) Evolution of the spectral region centered on the Fe II $\lambda\lambda$4924,5018,5169 lines during the rise to maximum light. The observed spectra are compared with SYNOW synthetic spectral calculations. The three vertical solid lines indicate the approximate wavelengths of this Fe II multiplet in the high velocity gas which is visible during the peculiar initial maximum in the $u'g'BV$ light curves. The three vertical dashed lines show the same multiplet at lower expansion velocity. Note that from day -27 through day -20, both velocity components are clearly present in the spectra. (right) Expansion velocity measurements for SN 2005bf. Values were estimated from SYNOW analyses of the observed spectra, and have typical errors of 500-1,000 km s^{-1}. The diamonds, triangles, and squares correspond to the high-velocity Fe II, Ca II, and Hα absorption, whereas the circles show the lower velocity Fe II and Ca II which we associate with the photosphere. The expansion velocities of the He I lines are plotted with an asterisk. The time axes are given in the observer's frame.

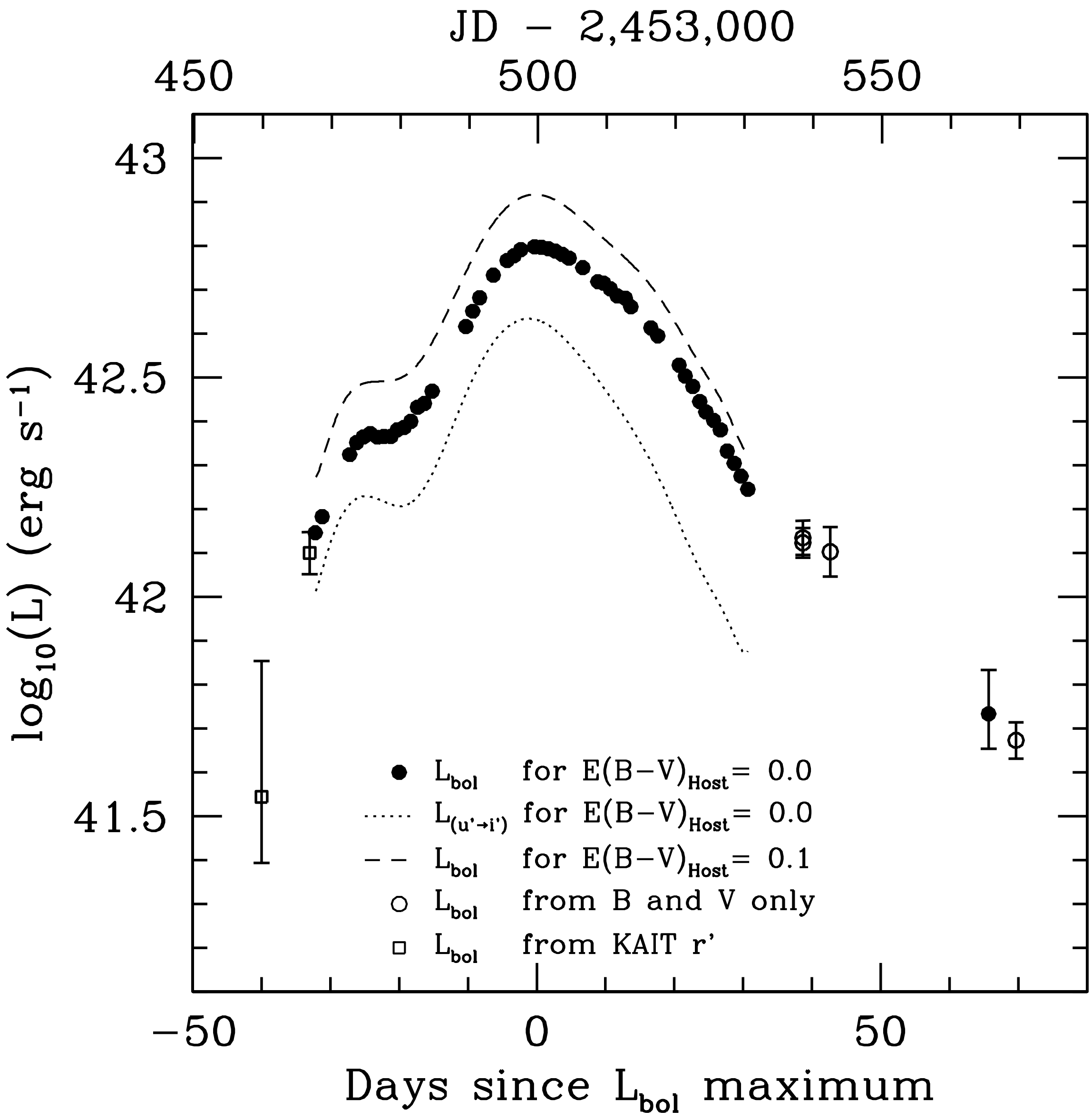

Fig. 8.— Bolometric light curve of SN 2005bf as derived from the optical photometry. Filled circles mark bolometric luminosities computed from integrated $u'g'r'i'BV$ fluxes, plus UV and IR corrections, $E(B-V)_{\rm Gal} = 0.045$ mag, $E(B-V)_{\rm Host} = 0.0$, and an assumed distance of 83.8 Mpc. Open circles mark bolometric luminosities derived from observed $(B - V)$ colors and bolometric corrections. Open squares mark luminosities derived from r' magnitudes measured on the discovery images of KAIT, and an extrapolation of the bolometric correction. The dashed line shows a smooth curve fit to the bolometric luminosities obtained assuming $E(B - V)_{\rm Host} = 0.1$. The dotted line shows a smooth curve fit to the uvoir luminosities $L_{u'\rightarrow i'}$ derived in the range of u' through i', and assuming $E(B - V)_{\rm Host} = 0.0$.

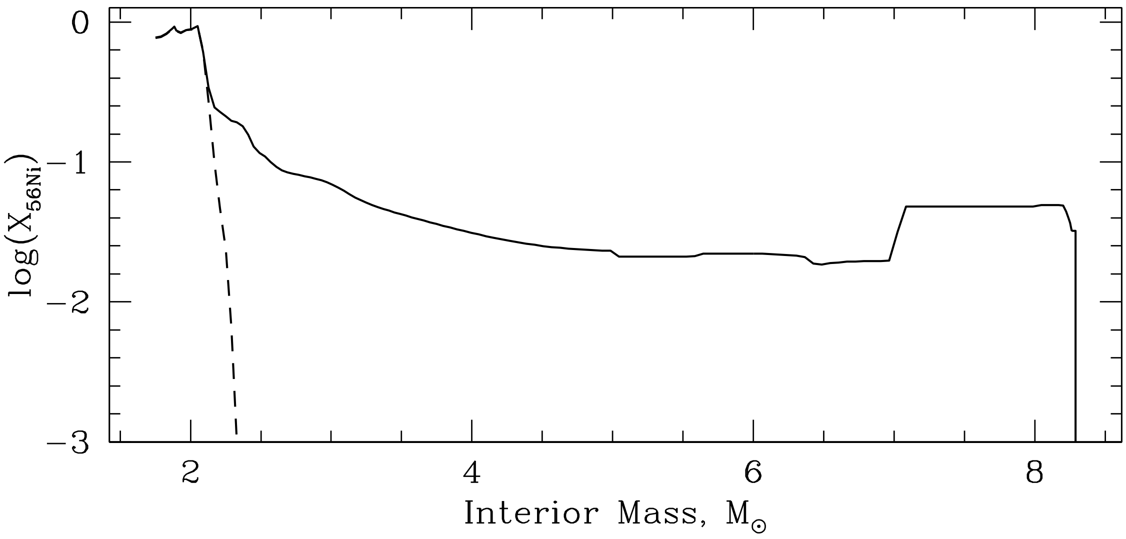

Fig. 9.— The distribution of the ^{56}Ni in the mixed (*solid line*) and unmixed (*dashed line*) versions of the 2×10^{51} erg explosion of an 8.29 $M_{\odot}$ WN star. The mass fraction of ^{56}Ni is plotted as a function of the interior mass in the star.

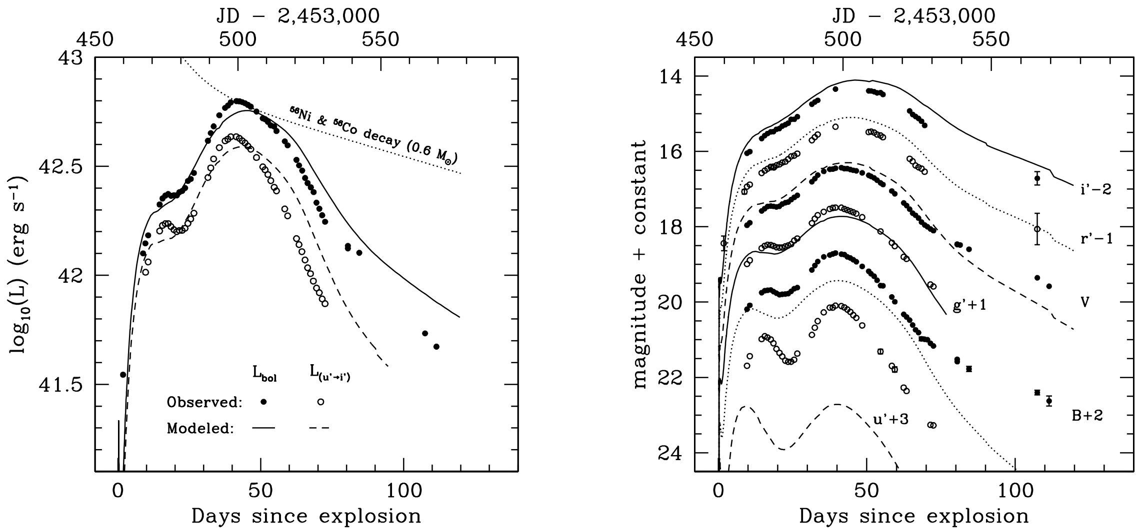

Fig. 10.— (left) The modeled bolometric (*solid line*) and uvoir (*dashed line*) luminosities of the mixed 8.29 M$_\odot$ WN star explosion. The circles mark the uvoir luminosity $L_{u'\to i'}$ (*open*), and the bolometric luminosity $L_{\rm bol}$ (*closed*), as derived from the observations. The dotted line shows the predicted luminosity if the ejecta were able to trap the whole gamma-ray output of 0.6 M$_\odot$ of radioactive ^{56}Ni produced in the explosion. The time of outburst was assumed as JD 2,453,458. (right) Modeled $u'g'r'i'BV$ light curves (*lines*) compared with the observations (*circles*).

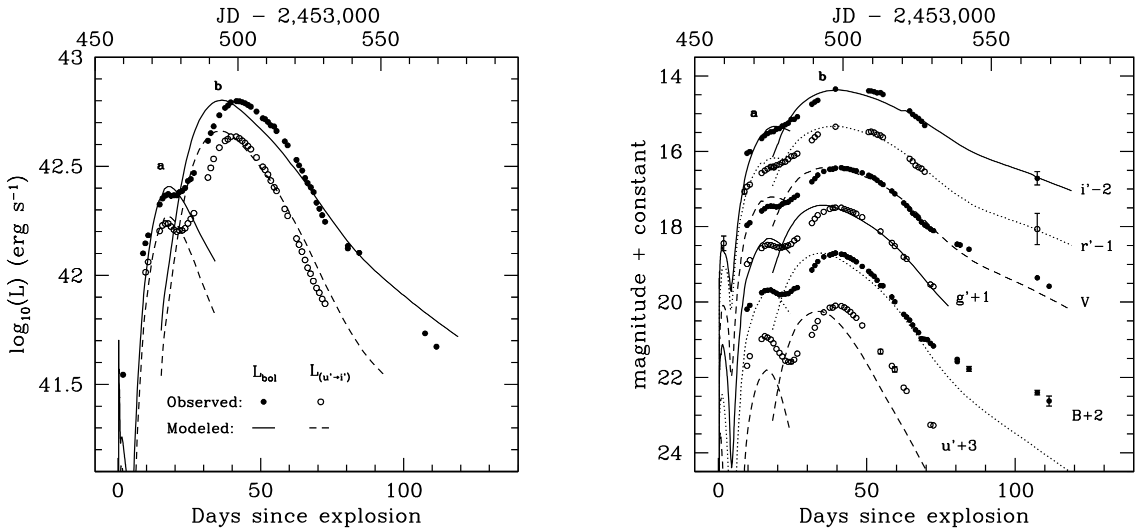

Fig. 11.— (left) The bolometric (*solid line*) and uvoir (*dashed line*) luminosities of a composite model made of two explosions: a) the 2×10^{51} erg explosion of 1.72 $M_\odot$ of helium and heavy elements containing 0.1 $M_\odot$ of ^{56}Ni, and b) the 2×10^{51} erg explosion of an 8.29 $M_\odot$ WN star. Neither model had mixed ^{56}Ni. The time of outburst was assumed as JD 2,453,458. Component a) is observable until about 20 days after outburst, when it is overrun by component b). (right) The contributions of components a) and b) to the $u'g'r'i'BV$ lightcurves (*lines*) compared with the observations (*circles*).